aerospace

MDPI

Article

Advanced Sizing Methodology for a Multi-Mode eVTOL UAV Powered by a Hydrogen Fuel Cell and Battery

Jae-Hyun An [1], Do-Youn Kwon [1], Kwon-Su Jeon [2], Maxim Tyan [2,*] and Jae-Woo Lee [1,*]

[1] Department of Aerospace Engineering, Konkuk University, Seoul 05029, Korea; tim0118@konkuk.ac.kr (J.-H.A.); imken45@konkuk.ac.kr (D.-Y.K.)
[2] Konkuk Aerospace Design-Airworthiness Research Institute (KADA), Konkuk University, Seoul 05029, Korea; kwonsu.jeon0125@gmail.com
* Correspondence: maxim@konkuk.ac.kr (M.T.); jwlee@konkuk.ac.kr (J.-W.L.)

Abstract: A critical drawback of battery-powered eVTOL UAVs is their limited range and endurance, and this drawback could be solved by using a combination of hydrogen fuel cells and batteries. The objective of this paper is to develop a sizing methodology for the lift+cruise-type eVTOL UAV powered by a hydrogen fuel cell and battery. This paper presents the constraints analysis method for forward flight/VTOL multi-mode UAV, the regression model for electric propulsion system sizing, a sizing method for an electric propulsion system and hydrogen fuel cell system, and a transition analysis method. The total mass of the UAV is iteratively calculated until convergence, and the optimization method is used to ensure that the sizing results satisfy the design requirements. The sizing results are the UAV's geometry, mass, and power data. To verify the accuracy of the proposed sizing methodology, the sizing and the conceptual design phase results of a 25 kg hydrogen fuel-cell-powered UAV are compared. All parameters had an error within 10% and satisfied the design requirements.

Keywords: UAV; eVTOL; multi-mode; hydrogen fuel cell; sizing; optimization

Citation: An, J.-H.; Kwon, D.-Y.; Jeon, K.-S.; Tyan, M.; Lee, J.-W. Advanced Sizing Methodology for a Multi-Mode eVTOL UAV Powered by a Hydrogen Fuel Cell and Battery. *Aerospace* **2022**, *9*, 71. https://doi.org/10.3390/aerospace9020071

Academic Editor: Peng Wei

Received: 19 October 2021
Accepted: 25 January 2022
Published: 27 January 2022

1. Introduction

Recently, the aviation industry has been attempting to incorporate electrification to solve various social problems. Electrification has been most developed in the field of UAVs (unmanned aerial vehicles) among various aviation industries, and many companies that develop and sell eVTOL (electric vertical take-off and landing) multi-copter drones, such as DJI, have appeared. However, with the current battery technology, multi-copter-type electric aircrafts have an endurance of up to 55 min (DJI MATRICE 300 RTK), and even electric multi-mode aircraft that can perform both forward flight (FF) and vertical take-off and landing (VTOL) to overcome the limitations of multi-copters have an endurance of only approximately 2 h (Penguin BE UAV). This endurance may be sufficient to carry out the mission, but to perform a greater variety of missions and increase the efficiency of the mission, technology that can overcome the current limitations is required. A hydrogen fuel cell (HFC) is one of the technologies developed to overcome this limitation, increasing the endurance through high specific energy. Table 1 compares the specific energy and specific power of the state-of-the-art battery technologies with those of the HFC system. According to a report by the Faraday Institute [1], the specific energy of the Tesla battery pack recently reached 270 Wh/kg, and NASA has set the specific energy to 400 Wh/kg as the future battery performance improvement goal for eVTOL aircrafts. In contrast, the HFC system has a higher specific energy of 1.7 kWh/kg [2]. Contrary to the specific energy, the specific power of the battery was higher than that of the HFC system. Therefore, although the HFC provides long endurance based on the high specific energy, it cannot be used in mission segments that require high power, and the battery can be used in VTOL missions that require large power based on the high specific power but cannot provide endurance.

Table 1. Specific energy and specific power comparison of Li-ion batteries and HFC systems.

	Specific Energy (Wh/kg)	Specific Power (W/kg)
Li-ion battery	270 [1]	1000 [2]
HFC system	1700 [2]	400 [2]

As the advantages and disadvantages of both batteries and HFCs are clear from the above analysis, to build a system that overcomes the limitations of the battery-only powered UAV, it is necessary to use the battery and HFC in a hybrid system. The propulsion system targeted in this paper was also an HFC–battery hybrid system, and a sizing methodology was developed considering its characteristics.

There are various ways in which the eVTOL UAV implements multi-mode flight. These can be represented by the lift+cruise type, vectored-thrust type, and tail-seater type as shown in Figure 1 below.

(**a**) (**b**) (**c**)

Figure 1. Various types of multi-mode aircrafts: (**a**) lift+cruise-type UAV, Mugin 350EV model [3]; (**b**) vectored-thrust-type UAV, Foxtech Nimbus VTOL V2 model [4]; (**c**) tail-seater-type UAV, Bell APT model [5].

Of these, the most used types are the lift+cruise and vectored-thrust types. This is because the tail-seater type has to change the direction of the entire UAV during transition; thus, the stability is lowered and there are fewer missions available. Both the lift+cruise and vectored-thrust types are suitable concepts for implementing multi-mode. The lift+cruise type has a disadvantage in that the VTOL propulsion system does not operate and acts as a drag force during FF flight, but this type is optimized for a wider range of missions, and the transition method is simple, so it is more commonly applied in UAVs [6]. Therefore, the UAV concept targeted in this paper was selected as a lift+cruise-type UAV.

Although various sizing methodologies for multi-mode UAVs powered by HFCs have been proposed, existing studies have several limitations. A study by Ng and Datta, which is the most similar to this paper, proposed a sizing method considering HFC–battery power sharing as well as an experimental study on the steady-state model and transient characteristics of the HFC and batteries [7]. In addition, the generation of the HFC polarization curve and the HFC sizing technique based on it are well described. Thirkell and Chen proposed a sizing method for a wide range of HFC systems presented through the consideration of various types of components [8]. Thomas suggested a multidisciplinary modeling and design environment that does not contain the assumption of a fuel-cell UAV [9]. However, since there is no sizing technique from the point of view of an aircraft, there is no method that considers the UAV's entire mission, and both the propulsion system sizing method based on the limited parameters given in the early design stage and the sizing method based on the design requirements are also insufficient. Therefore, our research team at Konkuk University has continuously been developing a sizing methodology from the perspective of the overall aircraft design process by improving the classical sizing methodology. The classical sizing method proposed by Raymer [10] and Roskam [11] considers the aircraft mission and the sizing method through the constraint analysis proposed by

Gudmundsson [12]. Maxim Tyan improved these classical sizing methods and developed the eVTOL UAV sizing methodology through consideration of multi-mode UAVs [13]. His methodology is a useful sizing tool in the early design stage, because it uses the design requirements as input, considers the entire mission performed by the UAV, and logically performs sizing using limited parameters. In addition, the sizing result obtained through this methodology satisfies the design requirements and is very accurate compared with the actual data from the developed UAV. However, his methodology was applied to a battery-only system, and a new sizing methodology is needed for a system using a hybrid HFC–battery system. In addition, the empirical method used in the propulsion system sizing should be updated.

Therefore, this paper proposed an improved methodology such that the previously developed eVTOL UAV sizing methodology can be applied to the hybrid HFC–battery system and can be accurately sized for the propulsion system by a regression model created using the latest propulsion system's performance data. The improved sizing methodology proposed in this paper uses only the limited parameters given in the early design stage, and the necessary assumptions are logically suggested. In addition, analysis of the transition mode, which is an important mission segment in multi-mode UAVs, is also included in the proposed sizing methodology to consider the transition requirements, stability, and required power. Sizing through the methodology proposed in this paper provides weight data including the weight of the UAV's propulsion system, power data for the entire mission segment, and geometry data of the main wing and propeller. These are all results that satisfy the design requirements through optimization and are sufficient to be used as data for conceptual and preliminary design, which is the next design stage.

2. Multi-Mode eVTOL UAV Concept

2.1. Multi-Mode UAV Operation Concept

For lift+cruise-type UAVs, FF and VTOL propulsion systems exist independently. Therefore, depending on the flight mode of the UAV, the propulsion system operates independently except when in transition mode. In transition mode, the FF and VTOL propulsion systems operate simultaneously. The VTOL propulsion system provides insufficient lift until the UAV achieves sufficient forward speed in the transition mode. However, they only operate together in this transition mode and do not share their functions. Therefore, the lift+cruise-type UAV can independently perform sizing of the FF and VTOL propulsion system.

Energy supply systems as well as propulsion systems are classified according to flight modes. The VTOL mode requires more power than the FF mode, but the mission time is shorter, so the energy required is less than that of the FF mode. Conversely, the FF mode requires less power than the VTOL mode but requires more energy than the VTOL mode because the mission time is longer. Therefore, it is necessary to apply an appropriate energy supply system for the flight mode of the UAV. Table 2 shows an appropriate energy supply system according to the power and energy required.

Table 2. Multi-mode UAV operation concept.

Mission	Power Required	Energy Required	Energy Supply System
Hovering	High	Low	Battery
VTOL	High	Medium	Battery
Transition	High	Low	Battery
Steady level flight	Low	High	HFC
Climb	Medium	High	HFC
Descent	Low	Low	HFC

2.2. Propulsion System Concept

Before sizing, it is necessary to define the type of propulsion system for the UAV, which is the main object of sizing. As mentioned earlier, the propulsion system targeted in this paper was a hybrid HFC–battery system and is configured as shown in Figure 2.

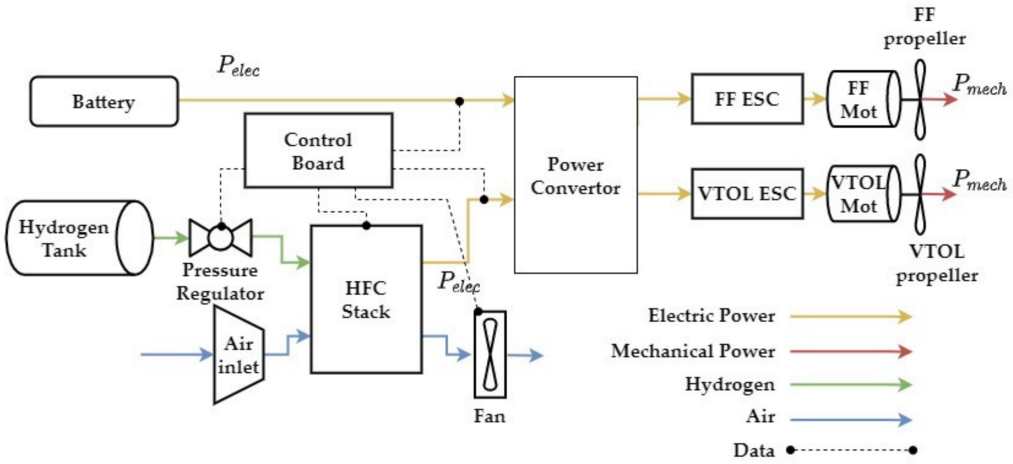

Figure 2. Multi-mode HFC eVTOL UAV propulsion system concept.

The HFC system consists of a hydrogen tank, an HFC stack that produces electricity, a regulator that ensures correct fuel flow to the stack, a control board that controls the entire system by receiving status information from pressure/temperature/current sensors, an air inlet, and a fan for maintaining the temperature of the stack. The battery exists independently of the HFC system and provides power. In addition, the lift+cruise-type UAV exists independently of the FF and VTOL electric branch that include the motor, electric speed controller (ESC), and propeller.

Since there are various types of each component constituting the UAV propulsion system and their characteristics are different, it is necessary to define a suitable type to be applied to the UAV. First, the hydrogen fuel cell selected was a proton exchange (or electrolyte) membrane fuel cell (PEMFC). Since the PEMFC is a hydrogen fuel cell with high technological maturity and operated at a low temperature of 30–100 °C, it is suitable for application to UAVs [14]. Air cooling is used as a method to maintain the temperature of the PEMFC, being suitable for UAVs with a power of under 5 kW [8]. For the hydrogen tank, a Type 4 tank was selected among the gaseous hydrogen tanks. Liquid hydrogen is 800 times less in volume and has higher energy density than gaseous hydrogen, but it must be kept at a low temperature, which limits its use in HFC UAVs [15]. The Type 4 tank is a structure in which a high-density plastic liner is wound with full carbon fiber, and it is used in hydrogen cars and aircrafts because it is light and durable. The battery selected was a Li-polymer (Li-po) battery, which is light, has high energy density, and is the main type used in UAVs. Table 3 summarizes the propulsion system targeted for sizing in this paper.

Table 3. Propulsion system configuration for the HFC eVTOL UAV.

Components	Type
Hydrogen fuel cell	PEMFC
Cooling method for HFC	Air cooling
Hydrogen tank type	Type 4 tank
Hydrogen tank pressure	300 bars
Hydrogen storage method	Gaseous hydrogen
Battery	Li-po battery
Motor	Brushless DC (BLDC) motor

3. Sizing Procedure

The sizing method proposed in this paper is performed as shown in Figure 3. Sizing is performed based on the design requirements through requirement analysis, the mission profile, and assumptions for sizing, and it predicts the weight, power, and geometry of the UAV.

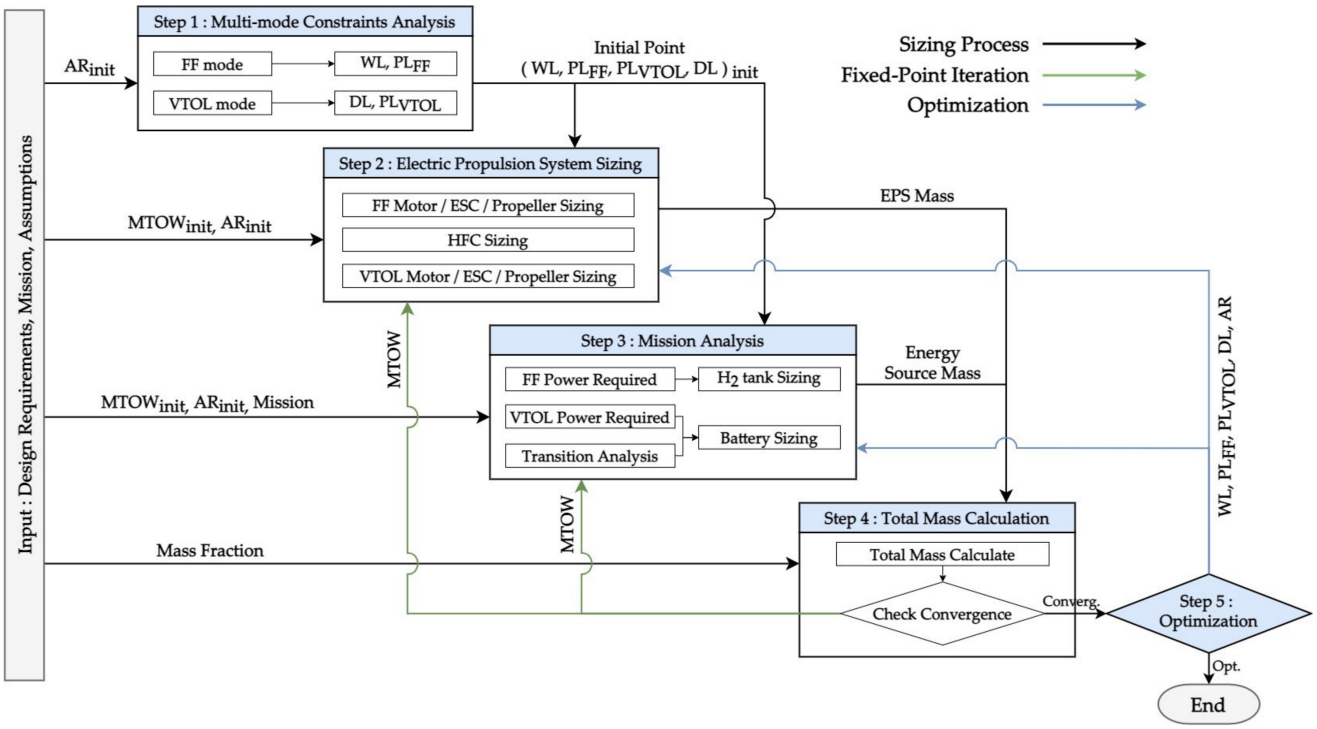

Figure 3. Sizing procedure.

The input for UAV sizing is the design requirements from the requirement analysis, the mission profile, which includes each mission segment's time, velocity, altitude, etc., and the assumptions for sizing. Multi-mode UAV sizing proceeds in the following order:

- **Step 1. Multi-Mode Constraints Analysis (MCA):** MCA is the stage in which the design area and the initial point are defined through sizing parameters, such as wing loading (*WL*), power loading (*PL*) and disk loading (*DL*), and the initial aspect ratio (*AR*), which is given from an assumption based on the performance constraints of the UAV for multi-mode that include the forward flight (FF) mode and the VTOL mode;
- **Step 2. Electric Propulsion System (EPS) Sizing:** EPS sizing is the stage of sizing the motor, ESC, propeller, and HFC. This step includes the estimation of not only the weight of the EPS but also the diameter of the propeller and the efficiency of the HFC;
- **Step 3. Mission Analysis:** This is the step of calculating the required power for each mission segment performed by the UAV and predicting the weight of the battery and hydrogen tank accordingly. This step includes an analysis of the transition segment;
- **Step 4. Total Mass Calculation:** This is the step of calculating the maximum take-off weight (MTOW) of the UAV by adding the weight and mass fraction of UAV components calculated through the EPS sizing and mission analysis. This step checks the tolerance of the calculated MTOW and repeatedly calculates the EPS sizing and mission analysis until the MTOW converges through fixed point iteration;
- **Step 5. Optimization:** This is the stage of optimizing the design point so that the sizing result can satisfy it by composing the optimization problem through the design requirements. The optimization objective function is to minimize the MTOW, and the design variables are wing loading, power loading, disk loading, and *AR*.

4. Multi-Mode Constraints Analysis (MCA)

The constraints analysis of general aircraft using internal combustion engines defines the design space using *WL* and the thrust-to-weight ratio (*TW*) as parameters. Therefore, the performance constraints are expressed in the form of $TW = f(WL)$. There are two differences between general constraints analysis and MCA. The first is that, since the aircraft targeted for sizing in this paper is an eVTOL UAV, the performance constraints are expressed as *PL* rather than *TW* as shown in Equation (1).

$$PL = \frac{(TW)V}{\eta_{prop}} \tag{1}$$

V is the speed in the direction of the UAV, and η_{prop} is the efficiency of the propeller. In this process, unlike normal piston engines, the EPS does not require a separate normalization because the performance of the motor does not change according to the air density. The second difference is that, as constraints for the VTOL mode are added, *DL*, which is a VTOL sizing parameter, is included in the sizing parameter, and FF *PL* and VTOL *PL* must be defined.

Since MCA has to define the design space, the performance requirements of the UAV should consist of the most critical conditions in the FF and VTOL modes. The most critical performance requirement means the condition that requires the most power and the requirements defined in Table 4 are the conditions that require the most power in the FF and VTOL modes, respectively.

Table 4. Performance constraints for multi-mode constraint analysis.

Flight Mode	Constraints
FF	Maximum speed level flight, maximum rate of climb, and stall speed
VTOL	Hovering, maximum speed take-off, and service ceiling

Equation (2) is an expression defining the *PL* constraints required when the UAV performs steady level flight at the maximum speed [12,16].

$$(PL)^{FF}_{level} = \eta_{prop} / \left(\frac{0.5\rho_0 V^3_{max} C_{D_0}}{(WL)} + \frac{2(WL)}{\rho_0 V_{max}(\pi e AR)} \right) \tag{2}$$

Here, C_{D_0}, is the minimum drag coefficient, and in the sizing corresponding to the initial design stage, it is assumed by comparing with the same class of UAV. Raymer [10] and Roskam [17] recommended 0.03 for propeller aircrafts, and Gudmundsson recommended 0.028–0.035 for fixed gear aviation aircrafts [12]. Since the multi-mode UAV has an additional motor boom and VTOL propeller, a higher value of 0.035 can be used. ρ_0 is sea level air density, and e is Oswald's span efficiency factor, which can by calculated using Equation (3) through AR [10].

$$\begin{gathered} e = 1.78\left(1 - 0.045 \times AR^{0.68}\right) - 0.64 \ : Straight - wing\ aircraft \\ e = 4.61\left(1 - 0.045 \times AR^{0.68}\right)(cos\Lambda_{LE})^{0.15} - 3.1 \ : Swept - wing\ aircraft \\ (\text{Where } \Lambda_{LE} > 30 \text{ deg}) \end{gathered} \tag{3}$$

For sweeps between 0 and 30, linearly interpolate between the results from the two equations [10]. When the UAV climbs at the maximum rate of climb (RoC), the *PL* constraints are defined as in Equation (4) [12,16].

$$(PL)^{FF}_{climb} = \eta_{prop} / \left(\frac{0.5\rho_0 V^3_c C_{D_0}}{(WL)} + \frac{2(WL)cos^2(\gamma)}{\rho_0 V_c(\pi e AR)} + V_c \sin(\gamma) \right) \tag{4}$$

Here, V_c is calculated as the airspeed in the direction of flight when climbing at the maximum RoC as in Equation (5), and γ is the climb angle of the UAV [12,17].

$$V_c = \sqrt{\left(\frac{2(WL)}{\rho_0}\right)\sqrt{\frac{k}{3C_{D_0}}}} \tag{5}$$

When performing level flight at stall speed, the constraint function is expressed as in Equation (6), which suggests the maximum value of WL. $C_{L_{max}}$ can be estimated by airfoil data.

$$(WL)^{FF}_{stall} = 0.5C_{L_{max}}\rho_0 V^2_{stall} \tag{6}$$

The performance constraints function of the VTOL mode is defined by axial momentum theory. In this case, it is difficult to calculate the parameters for the profile power in the initial design stage. Therefore, to account for these powers, the total required power is calculated using figures of merit (FoM). The FoM is the ratio of ideal induced power for a rotor in hover obtained from momentum theory and the actual power consumed by the rotor. Equation (7) shows the PL constraints required for the UAV to hover at ceiling [18,19].

$$(PL)^{VTOL}_{hover} = FoM/\sqrt{\frac{(DL)}{2\rho_0}} \tag{7}$$

Unlike hovering, when the UAV takes off vertically, climb power and parasite power are required in addition to induced power and profile power. Equation (8) shows the PL constraints required when the UAV takes off vertically at the maximum speed [18].

$$(PL)^{VTOL}_{takeoff} = \frac{1}{\frac{V_{takeoff}}{2} + \frac{1}{2}\sqrt{V^2_{takeoff} + \frac{2DL}{\rho_0}} + \frac{\rho_0 V^3_{tip}\sigma C_{d_{blade}}}{8DL} + \frac{\rho_0 V^3_{takeoff}}{DL} + \frac{\rho_0 V^3_{takeoff}}{S_{ratio}WL}} \tag{8}$$

Here, $C_{d_{blade}}$ is the average value of the profile drag of the UAV VTOL propeller's cross-section, and 0.01 can be used in the UAV [20]. σ is the solidity of the VTOL propeller, and it was assumed to be 0.077 with reference to the data of the existing T-motor VTOL UAV propeller. Figure 4a shows the solidity of the T-motor's multi-copter propellers by series [21].

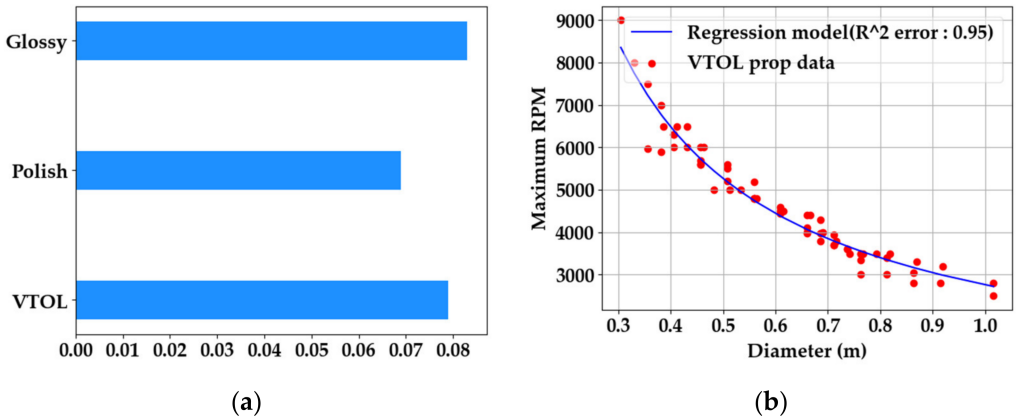

(**a**) (**b**)

Figure 4. VTOL propeller data: (**a**) the solidity ratio of the T-motor's VTOL propeller for each series [21]. The average value of solidity was 0.077; (**b**) the regression model for estimating the VTOL propeller's rpm according to the propeller diameter from the T-motor's VTOL propeller data [21]. The accuracy of the model was measured by the *R*-squared error, and the accuracy was high at 0.95. The unit of propeller diameter was in meters (m).

V_{tip} is the tip speed of the VTOL propeller and is calculated as in Equation (9). To assume the rpm, the maximum rpm data for each diameter of approximately 70 VTOL propellers of the T-motor were collected as shown in Figure 4b, and a regression model was made as shown in Equation (10) [21].

$$V_{tip} = \frac{\pi \times RPM \times D_{VTOL}}{60} \tag{9}$$

$$RPM = 2762.786 \times D_{VTOL}^{-0.932} \tag{10}$$

$V_{takeoff}$ is the vertical take-off speed, and S_{ratio} is the ratio of the total projected area of the UAV to the wing area, usually 1.3–1.4 [13]. Finally, in order to maintain the VTOL mode with a stability at high altitudes, the VTOL ceiling constraint was set in the service ceiling. The RoC at the service ceiling of a low subsonic aircraft is typically 0.5 m/s. To consider the safety margin in the service ceiling, the ratio of air density should be applied to Equation (8). The ratio of the air density at the service ceiling to the air density at sea level can be calculated as in Equation (11).

$$\sigma_{air} = \frac{\rho_{ceiling}}{\rho_o} \tag{11}$$

Figure 5 is an example of a multi-mode constraint diagram that visualizes the design space and design point as a graph through the previously defined constraint functions. The x-axis is PL, and the FF mode and VTOL mode share an axis on the graph, but the values are different at the design point, and the y-axis is WL in the FF mode and DL in the VTOL mode. In the example diagram, the blue area represents the design space of the FF mode, and the red area represents the design space of the VTOL mode. All points within the design space are feasible points, and the selection of design points was decided by the designer. Gudmundsson and other classical sizing methods suggest that design point at the constraint analysis should be to minimize wing area and required power [12]. In this paper, in the same context, the initial point for sizing was selected as a point that minimizes the wingspan and minimizes the FF/VTOL power, which is shown in Figure 5.

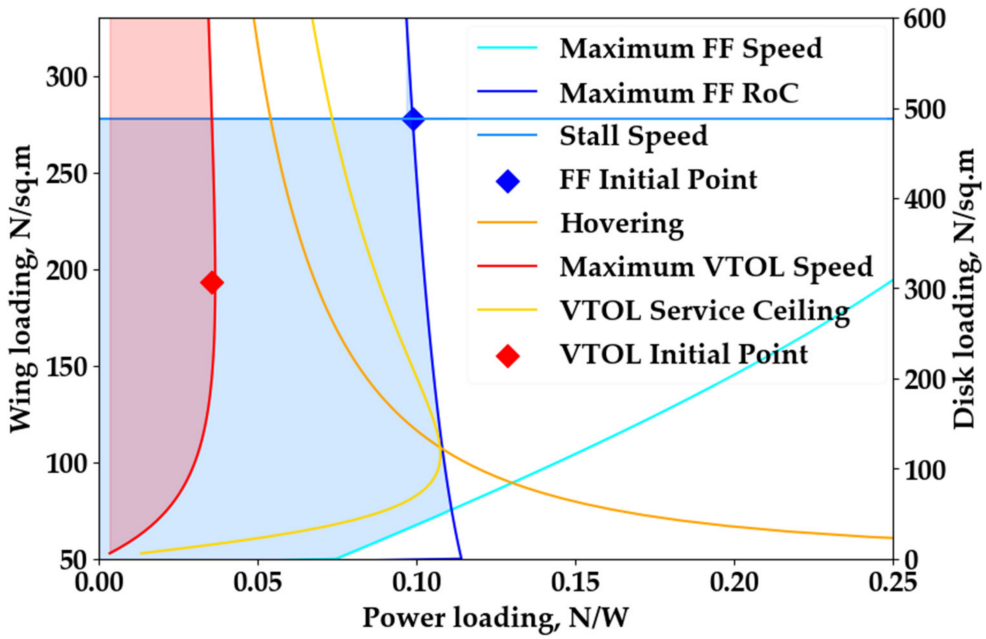

Figure 5. Example of multi-mode constraints diagram.

5. Electric Power System (EPS) Sizing

The EPS includes the motor, ESC, propeller, and HFC. Since only limited parameters are given during the sizing process, a regression model can be constructed based on the EPS data of the existing UAV, and sizing can be performed through this model. To construct the regression model, appropriate parameters should be selected, and the accuracy of the model should be verified by calculating the *R*-squared error. In this paper, the regression model was created through the "curve_fit" module of Python SciPy optimize [22].

5.1. Motor Sizing

Figure 6a,b are the regression model generated by collecting data from the products of the T-motor [21], Scorpion motor [23], and Hacker motor [24] which are representative UAV motor manufacturers.

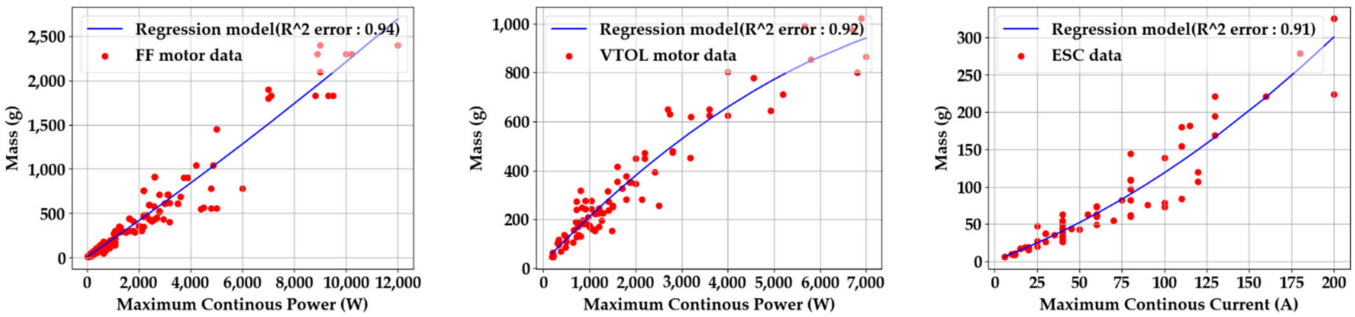

(**a**) (**b**) (**c**)

Figure 6. Motor and ESC regression model: (**a**) the model for FF motor sizing; (**b**) for VTOL motor sizing; (**c**) for ESC sizing. The motor data are from the T-motor [21], Scorpion motor [23], Hacker motor [24], and ESC data from the Hobbywing [25]. The accuracy of the model was measured by the *R*-squared error, and the accuracy was high at 0.94, 0.92, and 0.91, respectively. The regression model was generated by data from approximately 200 FF motors, 100 VTOL motors, and 70 ESCs. The unit of power is expressed in watts (W), the current in amperes (A), and the mass in grams (g).

Since the motors for the FF and VTOL have different characteristics, a regression model was also generated separately. The input for motor sizing uses the maximum power calculated through the *PL* defined in the MCA so that the motor can be operated without burn in all mission sections. Equations (12) and (13) are the regression models for sizing the FF and VTOL motors, respectively.

$$M_{mot.FF} = 0.196 \times 10^{-5} P_{max.FF}^2 + 0.201 P_{max.FF} + 5.772 \quad (12)$$

$$M_{mot.VTOL} = -0.922 \times 10^{-5} P_{max.VTOL}^2 + 0.196 P_{max.VTOL} + 23.342 \quad (13)$$

Here, the maximum power means electrical power, and it is a value that considers the efficiency of the motor from the mechanical power calculated through *PL*, and the efficiency of the motor is usually approximately 90–95%.

5.2. ESC Sizing

The ESC used for the eVTOL UAV is usually selected to accommodate the peak current required by the motor. Therefore, a regression model was built so that the maximum current divided by the maximum electric power by the rated voltage could be used as a sizing input. Figure 6c is the regression model generated by collecting data from the products of the Hobbywing [25]. In addition, Equation (14) is the regression model for sizing the ESC.

$$M_{ESC} = 0.324 \times 10^{-2} \left(\frac{P_{max.elec}}{U} \right)^2 + 0.847 \left(\frac{P_{max.elec}}{U} \right) + 1.532 \quad (14)$$

Here, U is the rated voltage used in the UAV, which is the same as the rated voltage of the battery.

5.3. Propeller Sizing

Propeller sizing predicts the diameter of the propeller and predicts the weight accordingly. The area of the VTOL disk can be calculated as in Equation (15) through the DL among the design variables defined by MCA. The area of the VTOL disk calculated here is the sum of the area of the entire disk, and the disk area of a single propeller must be divided by the number of VTOL propulsion systems.

$$A_{VTOL} = \frac{W}{DL} \tag{15}$$

Unlike the VTOL propeller, the FF propeller requires many variables to determine the diameter. The thrust and power generated by the FF propeller are determined by the diameter, pitch angle of propeller, forward speed, and rpm of the FF propeller. However, propeller sizing considering all these parameters in the early design stage is not possible. Therefore, the diameter of the propeller can be predicted by generating a regression model for the motor power and Kv, which means rpm per 1 volt and the most critical parameters in determining the diameter of the propeller. Figure 7 shows the regression model of the maximum power and Kv of the FF motor and the regression model of the appropriate diameter of the FF propeller according to the Kv of the motor.

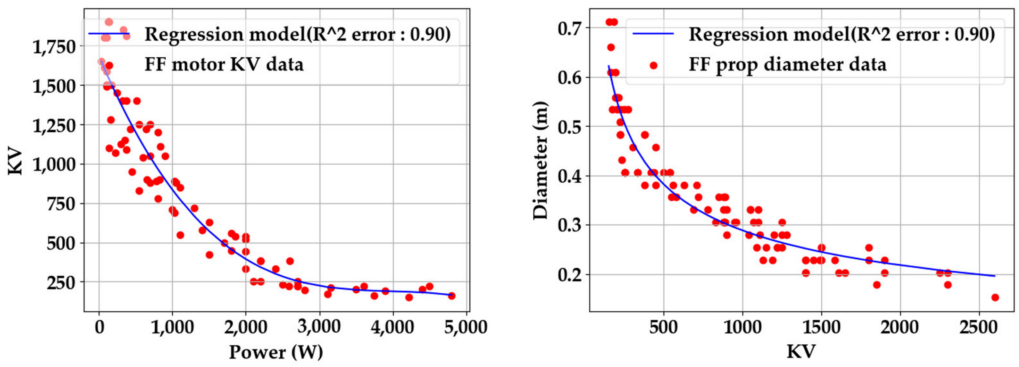

(**a**) (**b**)

Figure 7. Regression model to estimate the diameter of the FF propeller: (**a**) regression model for estimating the FF motor's Kv; (**b**) the regression model for estimating the FF's propeller diameter through the Kv. The FF motor's Kv data and appropriate propeller diameter data are from the T-motor [21] and Scorpion motor [23]. The unit of motor power is expressed in watts (W) and diameter of the propeller is in meters (m).

Equations (16) and (17) are regression models for estimating the FF motor Kv and FF propeller diameter.

$$Kv = -0.228 \times 10^{-7} \times P^3 + 0.0003 \times P^2 + -1.101 \times P + 1685.676 \tag{16}$$

$$D_{FF} = 4.735 \times Kv^{-0.405} \tag{17}$$

FF propellers and VTOL propellers have different pitch angles and structures due to the fact of their different operating characteristics; thus, the data on weight are also different. Therefore, the regression model for estimating the weight of the FF propeller and the VTOL propeller should be generated separately, and the regression model configured in Figure 8 is shown. For the FF propeller data, the APC propeller's data were referred to in [26], and for the VTOL propeller, the T-motor's propeller data were used [21].

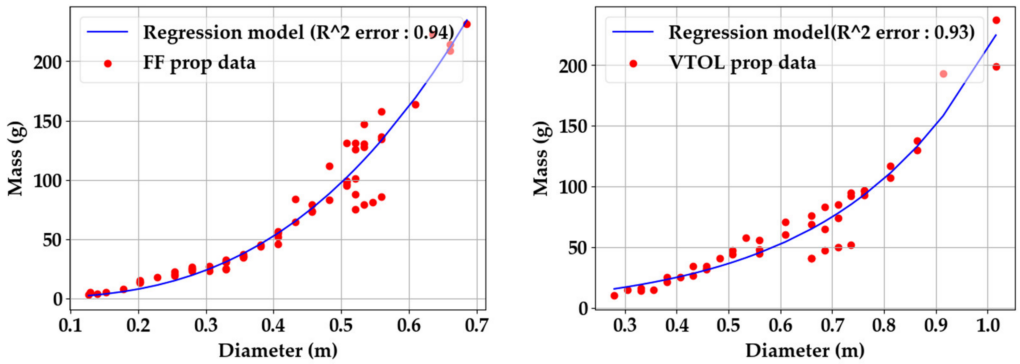

(**a**) (**b**)

Figure 8. Propeller regression model: (**a**) FF propeller regression model from APC propeller data [26]; (**b**) VTOL propeller regression model from T-motor propeller data [21]. The accuracy of the model was measured by the *R*-squared error, and the accuracy was high at 0.94 and 0.93, respectively. The unit of the diameter of the propeller is in meters (m), and mass of the propeller is in grams (g).

The regression model consists of the weight according to the diameter of the propeller, and Equations (18) and (19) are regression models for sizing of the FF propellers and VTOL propellers, respectively.

$$M_{prop.FF} = 670.644 * D_{FF}^{2.784} \tag{18}$$

$$M_{prop.VTOL} = 7.281 \times e^{3.389 * D_{VTOL}} - 3.232 \tag{19}$$

5.4. Electric Branch Mass Calculation

Through the results of the motor, ESC, and propeller sizing, the weight of the electric branch can be calculated as in Equation (20):

$$M_{eBranch} = f_{install}\left(n_{mot}\left(M_{mot} + M_{ESC} + M_{prop}\right)\right) \tag{20}$$

Here, $f_{install}$ is the weight of the parts necessary to mount the electric branch to the UAV, such as a motor mount and additional weight such as cables, and a value of approximately 1.2 is usually used [13].

5.5. HFC Sizing

In the existing HFC UAV sizing study, specific power was used for HFC sizing. This can be usefully used when there is no information about the HFC in the early design stage such as sizing. The Department of Energy (DOE) set a target of 0.85 kW/kg specific power for an 80 kW (net) integrated transportation FC power system operating on direct hydrogen [27]. Although this value is for a transportation application, the rated power is too large to be applied to a UAV, and the accuracy may not be high when applying it for sizing. Therefore, if the regression model was applied to the sizing through the HFC data currently used in the UAV, the weight can be predicted more accurately. Table 5 shows the rated power, system weight, specific power, and HFC system configuration of the HFC applied to the UAV developed by HES Energy [28], Intelligent Energy [29], and Doosan Mobility Innovation [30].

Table 5. HFC data from HES Energy Systems, Intelligent Energy, and Doosan Mobility Innovation.

HFC	Rated Power (W)	Weight (kg)	Specific Power (kW/kg)	HFC Configuration
HES Aerostak A-250 [28]	250	0.72	0.35	Stack+Control+Case+Fan+Li-po battery
HES Aerostak A-500 [28]	500	1.3	0.38	Stack+Control+Case+Fan+Li-po battery
HES Aerostak A-1000LV [28]	1000	2.036	0.49	Stack+Control+Case+Fan+Li-po battery
HES Aerostak A-1000HV [28]	1000	1.8	0.56	Stack+Control+Case+Fan+Li-po battery
HES Aerostak A-1500 [28]	1500	3	0.50	Stack+Control+Case+Fan+Li-po battery
HES Aerostak A-2000 [28]	2000	4	0.50	Stack+Control+Case+Fan+Li-po battery
Intelligent Energy IE-Soar 650 [29]	650	1.19	0.55	Stack+Control+Case+Fan+Li-po battery
Intelligent Energy IE-Soar 800 [29]	800	1.38	0.58	Stack+Control+Case+Fan+Li-po battery
Intelligent Energy IE-Soar 2.4kW [29]	2400	5.62	0.43	Stack+Control+Case+Fan+Li-po battery
Doosan DM/DP15 Powerpack [30]	1250	2.9	0.43	Stack+Control+Fan+Li-po battery

Using this data, a regression model for the weight according to the rated power of the HFC applied to the UAV can be generated as shown in Figure 9a and Equation (21).

$$M_{HFC} = 0.423 \times 10^{-3} \times P_{req}^2 + 1.08 \times P_{req} + 451.651 \quad (21)$$

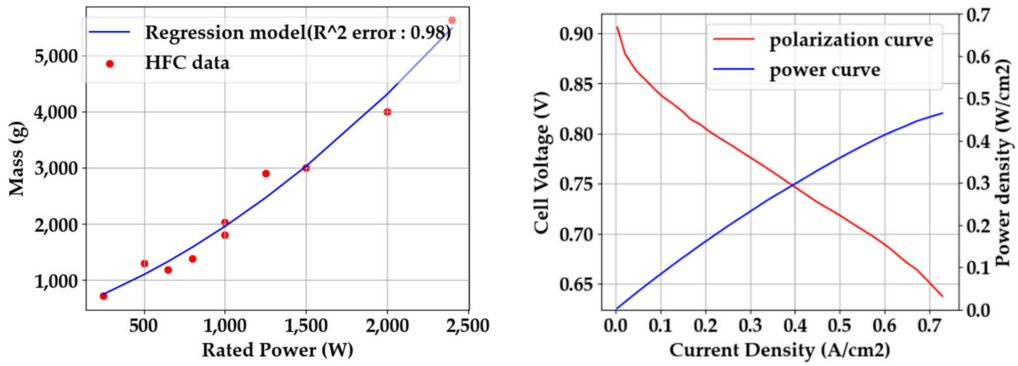

(**a**) (**b**)

Figure 9. (**a**) Regression model for HFC sizing. The accuracy of the model was measured by the *R*-squared error, and the accuracy was high at 0.98. The unit of rated power is expressed in watts (W), and the mass of the HFC in grams (g). (**b**) Examples of a polarization curve and power curve.

Using the regression model of Equation (21), it is possible to predict the weight reflecting the current technology level for the HFC applied to the UAV having the same configuration as in Table 5. However, since not all HFCs have the above configuration, in this paper, another method for sizing the HFC based on the single-cell performance of the HFC is presented.

The polarization curve is a curve showing the trend of current density and voltage of a single HFC cell and is used to test the performance of that single cell. If the polarization curve is used, sizing can be performed based on the performance of the HFC to be applied to the UAV. The method of generating the polarization curve has been suggested through various references, and it can be generated in various ways [2,7,31]. Figure 9b is an example of a polarization curve of the HES AEROSTAK 200W model [2,28].

In Figure 9b, the power curve is a curve showing the trend in power density, which is multiplied by the current density and voltage. When the polarization curve is prepared, the number of cells constituting the HFC stack can be predicted as in Equation (22):

$$n_{cell} = \frac{V_{design}}{V_{cell}} \quad (22)$$

Here, V_{design} is the voltage of the HFC given in the design requirements, and V_{cell} is the voltage of a single cell that maximizes the power density of the cell. If the number of cells in the HFC is determined, the electrode area of a single cell can be determined as in Equation (23). The electrode area means the area where the actual chemical reaction takes place.

$$A_{cell} = \frac{P_{req}}{p_{cell} n_{cell}} \tag{23}$$

Here, p_{cell} is the power density of a single cell. The weight of the HFC can be predicted as in Equation (24) using the previously calculated information of the single cell [7].

$$M_{HFC} = \frac{n_{cell} k_A \rho_{cell} A_{cell}}{1 - \eta_{OW}} (1 + f_{BOP}) \tag{24}$$

Here, ρ_{cell} is the area density of a single cell, and Wanyi NG recommends 1.57 kg/m^2 [7]. k_A is the ratio of the cross-sectional area to the electrode area of a single cell, and four is used as a conservative value. η_{OW} is 0.3 as the overhead fraction for gaskets, seals, connectors, endplates, etc., constituting the HFC stack [7]. f_{BOP} is the ratio of the BOP weight to the HFC weight, and this value is different depending on the HFC configuration. In this paper, 0.2 was used in the case study.

One of the important parameters for prediction in HFC sizing is the efficiency of the HFC. At the current technology level, the efficiency of the PEMFC is approximately 40–50%, and if there is no information about the polarization curve of a single cell, this value can be used for sizing [14]. However, when the polarization curve is defined, the efficiency of the HFC can be calculated as in Equation (25) [32]:

$$\eta_{HFC} = \frac{2F * P_{req}}{\Delta H * i_{FC}} \tag{25}$$

Here, F is a Faraday constant of 96,485.4 C/mol, and ΔH is a chemical reaction energy of 284,000 J/mol. P_{req} is the electrical power required by the mission operated by the HFC, and the efficiency of the HFC decreases as the required power increases.

6. Mission Analysis

6.1. Required Power Analysis

Mission analysis is the stage of predicting the amount and weight of fuel that enables the UAV to perform the mission given in the mission profile and analysis of transition segment. For this, it is first necessary to define the power required for each mission segment. However, this was defined in the form of $PL = f(WL)$ or $PL = f(DL)$ in the MCA stage, and it can be transformed into a formula that defines the actual power. Therefore, the power required for each mission segment can be defined through the power loading constraints defined by the MCA and MTOW given for each iteration in the multi-mode sizing loop.

6.2. Transition Analysis

The purpose of transition analysis is to predict the power and time required for transition for sizing a battery or hydrogen tank. The transition time of a multi-mode UAV is relatively short compared to other missions and consumes less fuel, so it may not be sensitive to battery or hydrogen tank sizing. However, since the transition time and transition stability act as important design requirements, they should be considered from the early design stage. The lift+cruise-type UAV's transition mechanism is relatively simple compared to the tilting mechanism, but calculating the transition time and power required still requires complex analysis. Therefore, sizing simplifies this process with a few assumptions. These assumptions must be logical and ensure the transition stability of the UAV. The transition method can take various strategies, such as maintaining the altitude, transitioning by accelerating through gliding at the beginning of the transition, or transitioning while

climbing. This paper deals with the transition method while maintaining the altitude. The assumptions for transition analysis in this paper are as follows:

1. During the transition, all control of the UAV is handled by the flight control computer (FCC) automatically;
2. During the transition, the altitude is kept constant by the FCC that maintains the sum of the lift generated from the wing and the thrust generated from the VTOL propulsion system to be the same as the weight;
3. For transition stability, the UAV starts the transition after maintaining the hovering state for a few seconds;
4. For transition stability, the UAV terminates the transition when the forward flight speed reaches 1.2 times the stall speed, and at the end of the transition, the UAV maintains the trim;
5. For transition stability, FCC provides a guide control in which the lift sharing between the wing and VTOL thrust can be switched smoothly;
6. For transition stability, the transition time should be minimized by holding the FF throttle at 100% until forward flight speed reaches stall speed.

These assumptions make it possible to perform a transition analysis using the parameters given in the sizing step, while ensuring the stability of the transition. Through the above assumptions, the conditions for the start and end of the transition mode can be summarized as shown in Table 6.

Table 6. Starting and terminal condition of the transition mode of multi-mode UAVs.

Parameter	Starting Condition	Terminal Condition
V_∞	0 m/s	$1.2 \times V_{stall}$
L_{wing}	0 N	W
T_{FF}	0 N	D
T_{VTOL}	W	0 N
$Lift\ Sharing$	100%	0%

For transition analysis, force equilibrium should be defined during transition, and free body diagrams are used for this. Figure 10 shows the free body diagram of UAVs during the transition mode.

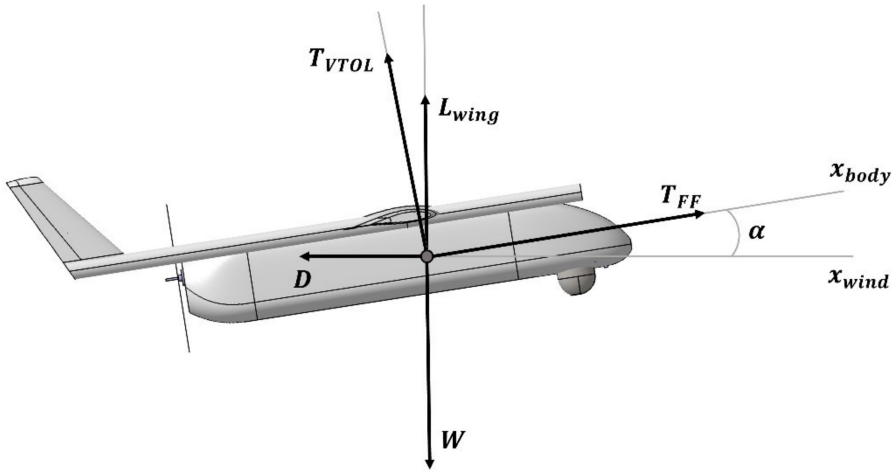

Figure 10. Lift+cruise UAV's free body diagram during transition mode.

Here, L_{wing} is lift generated by the wing of the UAV, D is the drag, W is the weight of the UAV, α is angle of attack of the UAV, T_{FF} is the thrust which is generated by the forward flight propulsion system, and T_{VTOL} is thrust which is generated by the VTOL propulsion system. Since the forward speed is low during transition, sufficient lift can be

obtained considering the angle of attack of the UAV, and the lift coefficient according to the angle of attack can be predicted through the lift curve of the airfoil. Through the second assumption for transition analysis and the free body diagram, the z-direction force can be calculated as in Equation (26):

$$\sum F_Z = W - L_{wing} - T_{FF} \times sin(\alpha) - T_{VTOL} \times cos(\alpha) = 0 \tag{26}$$

In addition, through the free body diagram, the x-direction force and forward acceleration are calculated as in Equation (27):

$$a_x = \frac{F_x}{m} = \frac{T_{FF} \times cos(\alpha) - D - T_{VTOL} \times sin(\alpha)}{m} \tag{27}$$

The lift from the wing in Equation (26) can be calculated from the fifth assumption for transition analysis. The guide control of lift sharing can be defined according to the operating conditions, and in this paper, it is defined in the form of a simple sine curve as shown in Equation (28):

$$\begin{aligned} d = \frac{(W - L_{wing})}{W} &= \frac{(W - q_\infty C_{L_{req}} S_{wing})}{W} \\ &= 0.5\left(\sin\left(\frac{\pi}{1.2 \times V_{stall}} \times V_\infty - \frac{3\pi}{2}\right) + 1\right) \end{aligned} \tag{28}$$

Here, d is lift sharing and is expressed as a percentage of W, and $C_{L_{req}}$ is required lift at that time. Since the forward speed is small at the beginning of the transition, a lift coefficient higher than the lift coefficient at the stall angle of attack may be required to generate the lift required by the guide control. In this case, $C_{L_{req}}$ can be replaced by $C_{L_{max}}$ at the stall angle of attack of UAV and the guide control should be modified. According to the sixth assumption for transition analysis, the forward flight thrust is maintained as the maximum thrust before the stall speed and decreases linearly to match the drag force from the stall speed until the transition is terminated. Figure 11a shows an example of lift sharing according to the forward velocity of a UAV during the transition mode. The blue line shows the original guide control of lift sharing, and the yellow line shows the modified lift sharing profile due to the insufficient forward speed at the beginning of the transition. In addition, Figure 11b shows the example of forward thrust according to the forward velocity of a UAV during transition mode.

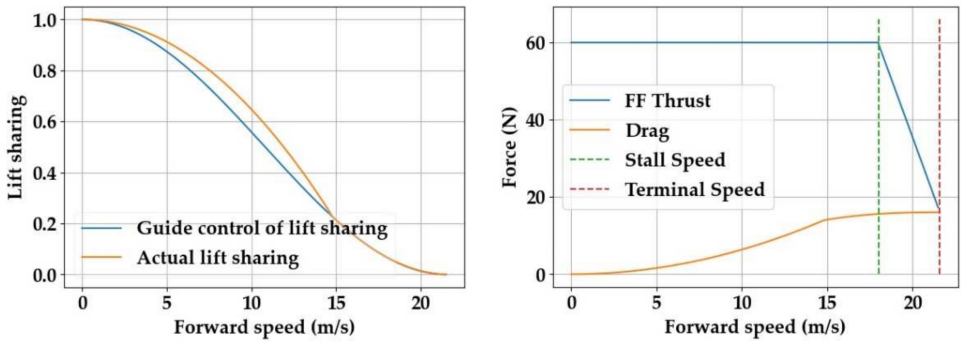

(**a**) (**b**)

Figure 11. (**a**) An example of lift sharing guide control according to the forward velocity of a UAV during transition mode. (**b**) An example of forward thrust and drag according to the forward velocity of a UAV during transition mode.

Through the above process, the force acting on the UAV, the change in forward speed, and the transition time in the transition segment can be calculated, and the required power can be calculated and used for battery sizing. The re-transition process from the FF mode

to the VTOL mode can also be analyzed by applying the starting and terminal conditions in reverse through the above assumptions.

6.3. Li-po Battery Sizing

In the case of Li-po batteries for eVTOL UAVs, the battery's capacity and rated voltage have the most sensitivity on the battery's weight. Therefore, the battery sizing technique considering the capacity and rated voltage guarantees an accurate estimation of the battery weight. Batteries with the rated voltage of 6S–12S (22.2–44.4 V) are most commonly used. Therefore, there are many 3S (11.1 V), 4S (14.8 V), and 6S (22.2 V) battery products on the market, and a higher rated voltage can be produced through their series connection. A regression model for battery sizing was created from the data of 3S, 4S, and 6S batteries. The capacity (mAh) of the battery must be determined to provide the energy required for the mission performed by the UAV. Using the power required for each mission segment defined through the method presented in Section 6.1 and the mission time presented in the mission profile, the required capacity of the battery can be calculated using Equation (29):

$$C_{req} = \frac{\left(\sum_{i=1}^{n_{seg}} \frac{P_{req.i}}{\eta_{mot}} \times t_i\right)}{U_{rated}\eta_{batt}f_{usable}} \tag{29}$$

Here, f_{usable} is a factor to prevent voltage drop when the battery is discharged for a long time, and approximately 0.85 is usually used, and U_{rated} is the Li-po battery's rated voltage. In this process, depending on the decision of the designer, it is also possible to calculate the required energy by giving a margin from the total mission time given in the mission profile. After the required energy of the battery is defined, the weight of the battery can be predicted using the regression model in Figure 12 [33].

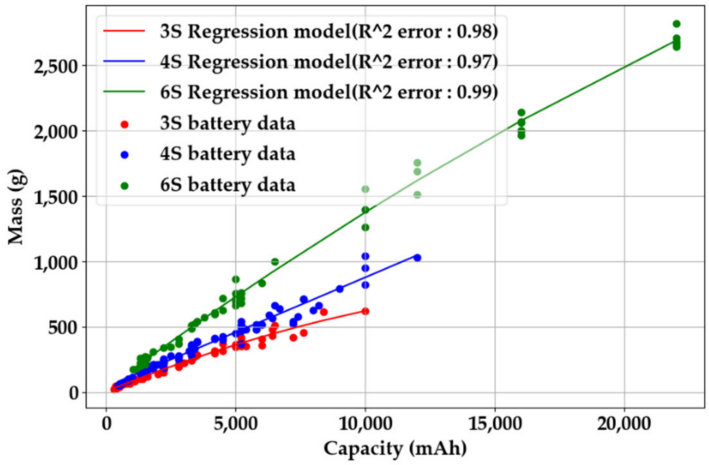

Figure 12. Regression model of a Li-po battery. The accuracy of the model was measured by the *R*-squared error, and the accuracy was high at 0.98, 0.97, and 0.99. The unit of capacity of the battery is expressed in mAh, and mass of the battery in grams (g).

The regression model for 3S, 4S, and 6S Li-po battery sizing is as in Equation (30):

$$\begin{cases} 3S(11.1V) \ : M_{batt} = -0.019 \times 10^{-4} C_{req}^2 + 0.08 C_{req} + 7.864 \\ 4S(14.8V) \ : M_{batt} = 0.83 \times 10^{-7} C_{req}^2 + 0.083 C_{req} + 45.352 \\ 6S(22.2V) \ : M_{batt} = -0.116 + \times 10^{-5} C_{req}^2 + 0.147 C_{req} + 27.827 \end{cases} \tag{30}$$

6.4. Hydrogen Tank Sizing

Hydrogen tank sizing starts with defining the required electrical power for each mission segment, the same as battery sizing. However, the difference from battery sizing is that the efficiency of the fuel cell according to the power required in the mission segment is

included in the sizing. The method of calculating the fuel cell efficiency has already been described in Equation (25). When the required power for each mission section and the fuel cell efficiency are calculated, the hydrogen consumption (HC) can be calculated as shown in Equation (31):

$$HC = \frac{P_{req}}{LHV \times \eta_{fc}} \tag{31}$$

Here, the unit for HC is g/h, which indicates the amount of hydrogen consumption per unit time, and LHV is the low heating value of hydrogen, which is 33.3 Wh/g. If the hydrogen consumption for each mission segment is calculated, the amount of hydrogen required for the entire mission is calculated according to Equation (32) through the mission time given in the mission profile.

$$m_{H_2} = \sum_{i=1}^{n_{seg}} HC_i \times t_i \tag{32}$$

A regression model that can estimate the weight and volume of a hydrogen tank based on the amount of hydrogen required was generated as shown in Figure 13. The regression model was constructed based on the data of Type 3 and 4 tanks [29], and this can be expressed as Equations (33) and (34).

$$M_{tank} = 19.068 \times m_{H_2}^{0.8215} \tag{33}$$

$$V_{tank} = 4.63 \times m_{H_2}^2 + 45.782 \times m_{H_2} + 0.102 \tag{34}$$

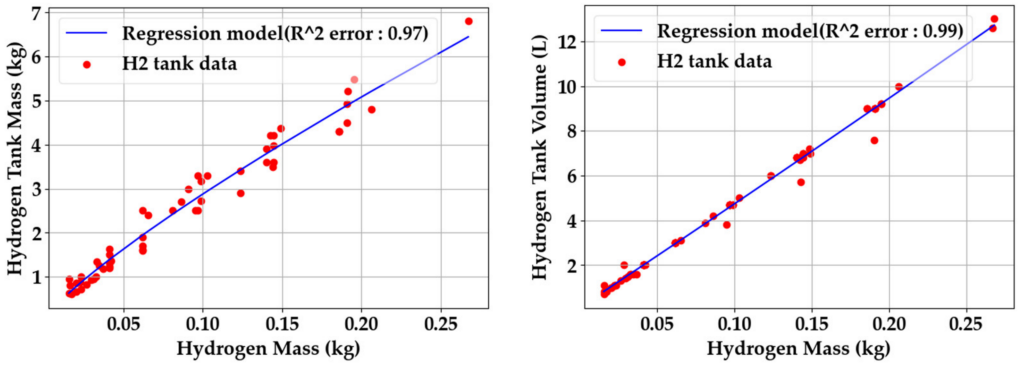

(**a**) (**b**)

Figure 13. Hydrogen tank regression model: (**a**) hydrogen tank weight regression model; (**b**) hydrogen tank volume regression. The accuracy of the model was measured by the *R*-squared error, and the accuracy was high at 0.97 and 0.99, respectively. The unit of mass for the hydrogen and the tank is in kg, and volume of the tank is in L.

7. Total Mass Calculation

The MTOW of the UAV is the most important parameter among the results of sizing and is calculated by adding up the weights of the components comprising the UAV calculated in the previous section. The total mass calculation was calculated through fixed point iteration, which is iteratively calculated until the MTOW converges below a predefined tolerance. The first iteration uses the initial MTOW given in the design requirement. For those of the components constituting the UAV that can be calculated, the actual value was added to the total weight through the methods presented above, and the remainder was calculated as the mass fraction, which is the ratio of the total weight [13]. The items for which the mass fraction should be assumed are the air frame, avionics, and subsystem. For the air frame weight, it is recommended to use a mass fraction of 25–35% for the FF

UAV as an initial estimation in sizing and 5% for the avionics [34]. The mass fraction of the subsystem varies depending on the operation type of the UAV, which is 5–7% for UAVs designed for delivery and 15% for advanced surveillance equipment [13]. The total weight of the multi-mode HFC eVTOL UAV was calculated as in Equation (35):

$$MTOW = \frac{M_{propulsion}^{FF} + M_{propulsion}^{VTOL} + M_{FC.sys} + M_{batt} + M_{payload}}{1 - (MF_{frame} + MF_{subsys} + MF_{avionics})} \quad (35)$$

Here, $M_{FC.sys}$ is the weight of the entire hydrogen system, including the previously calculated HFC, tank, regulator, and control board. The calculated MTOW is used as a value for fixed-point iteration in the multi-mode sizing loop, and the multi-mode sizing loop is repeatedly calculated until the MTOW converges.

8. Optimization

Since the design point selected in the MCA was selected within the design space that satisfied the performance constraints of the UAV, it is not known whether it satisfies the design requirements other than the performance constraints. Previous sizing techniques used graphical techniques, such as carpet plots, to obtain results that satisfy the design requirements. However, it is difficult to quantitatively and efficiently find the optimal point. Therefore, in this paper, a method for defining a design point that satisfies the design requirements through a numerical optimization algorithm was developed. The objective function of the optimization is to minimize the MTOW of the UAV, and the constraint is a design requirement including the performance constraint defined in the MCA. The design variables are wing loading, FF/VTOL power loading, disk loading, and AR, which are key parameters for multi-mode UAV sizing. Table 7 is an example of an optimization formulation. The optimization algorithm used in this paper was Python's SciPy SLSQP [22]. It is suitable for solving nonlinear optimization problems with constraints, and for sizing problems in the early design stage, because the computation time is shorter than other global optimization algorithms.

Table 7. Example of sizing optimization formulation.

	Variable		Value
Minimize:	MTOW		
Subject to:	Maximum FF speed	$\geq$	30 m/s
	Maximum RoC	$\geq$	6 m/s
	Stall speed	$\leq$	18 m/s
	VTOL ceiling	$\geq$	1000 m
	Maximum take-off speed	$\geq$	10 m/s
	Hydrogen fuel system mass	$\leq$	10 kg
	Wingspan	$\leq$	3.5 m
	FF propeller diameter	$\leq$	30 inches
	VTOL propeller diameter	$\leq$	30 inches
	Transition time	$\leq$	30 s

9. Case Study

The sizing methodology proposed in this paper was implemented in the 25 kg hydrogen fuel cell UAV design project. The quantitative goals were an MTOW under 25 kg, endurance up to 6 h, a hydrogen system mass under 10 kg (40% mass fraction), and continuous power of the HFC up to 2 kW. As a design process before sizing, requirements analysis and concept selection were performed. Table 8 shows the design requirements derived through the requirements analysis, and the concept of operation for this UAV was surveillance. Figure 14 shows the mission profile of the surveillance HFC UAV.

Table 8. The 25 kg hydrogen fuel cell UAV design requirements.

Requirements	Value	Remarks
MTOW	<25 kg	
Endurance	>6 h	
HFC system mass	<10 kg	
Payload mass	1.25 kg	Camera for surveillance
HFC maximum continuous power	>2 kW	
Wingspan	<3.5 m	Market analysis
Cruise altitude	150 m	FAA requirement 400 ft
Maximum speed	>35 m/s	Market analysis
Cruise speed	25 m/s	Market analysis
Stall speed	<18 m/s	Market analysis
Maximum RoC	>6 m/s	Market analysis
Maximum take-off speed	>10 m/s	Market analysis
VTOL service ceiling	1000 m	Market analysis
FF propeller diameter	<30 inches	Available size for regression
VTOL propeller diameter	<30 inches	Available size for regression
Transition time	<30 s	Market analysis

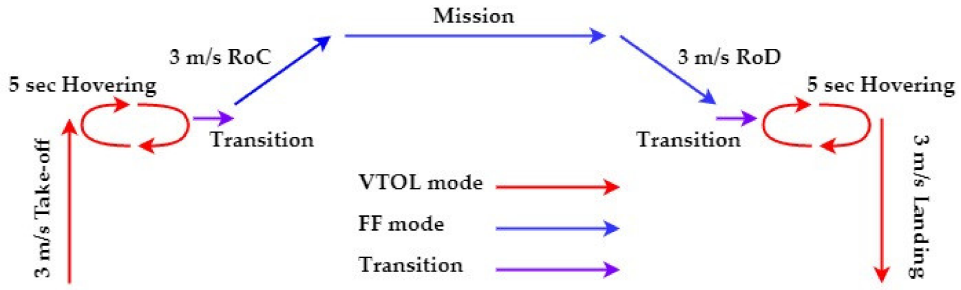

Figure 14. The 25 kg multi-mode surveillance HFC UAV mission profile.

The results of the sizing are compared with the conceptual design results of the UAV to validate the accuracy of the methodology. An integrated analysis and configuration optimization of the UAV were performed with the Konkuk University in-house program ADSP (Aircraft Design and Synthesis Program). ADSP can perform multi-disciplinary analyses and optimizations of UAVs as well as very light aircrafts (VLAs), UCAVs, and electric aircrafts, and its accuracy and efficiency have been verified [35–37]. In addition, CFD for high-fidelity aerodynamic analysis and wind tunnel experiments for obtaining high-fidelity electric propulsion system performance data were performed to construct high-fidelity analysis data and, thus, the design results are very accurate. The HFC stack and BOP were designed by Nexcoms Co., Ltd., and the HFC sizing result was verified through the data of the developed product [38]. The conceptual design process through ADSP proceeded as shown in Figure 15. Based on the sizing result, the propulsion system was selected, components placement performed, and then the conceptual design was carried out through multi-disciplinary integrated analysis and optimization.

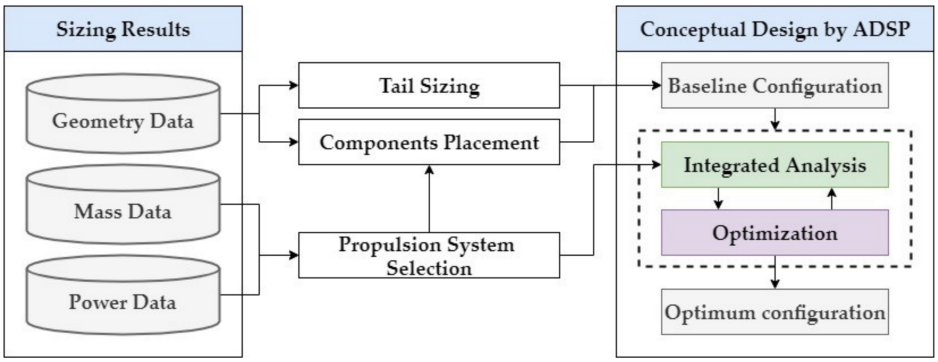

Figure 15. Conceptual design process through ADSP.

9.1. Optimum Sizing Result

Table 9 shows a comparison between the sizing result and the conceptual design result. Initial sizing refers to the sizing result at the initial design point selected by the designer before optimization, and optimum sizing refers to a design point that satisfies the design requirements through optimization.

Table 9. Comparison of initial point, sizing results, and conceptual design results.

Parameter	Unit	Initial Point	Sizing Results	Conceptual Design Results	Error (%)
MTOW	kg	40.923	24.909	24.990	0.325
Wing loading	N/m^2	277.842	259.226	252.890	2.505
FF power loading	N/W	0.099	0.102	0.095	7.447
VTOL power loading	N/W	0.035	0.035	0.032	9.078
Disk loading	N/m^2	360.777	250.749	249.904	0.338
AR	.	10.0	13.0	12.295	2.795
Wing area	m^2	1.444	0.942	0.969	2.795
Wingspan	m	3.801	3.5	3.452	1.379
Endurance	hours	6.0	6.0	6.062	1.023
FF propeller diameter	inch	20.864	19.621	20.0	1.895
VTOL propeller diameter	inch	25.405	21.924	22.0	0.346
Airframe mass fraction	.	0.35	0.35	0.359	2.507
Fuel cell system mass	kg	22.826	9.403	9.950	5.497
HFC mass	kg	5.516	3.254	3.0	8.483
Cylinder mass	kg	9.789	5.599	5.4	3.677
Battery mass	kg	1.876	1.115	1.15	3.039
FF propulsion system mass	kg	1.374	0.804	0.87	7.563
VTOL propulsion system mass	kg	3.102	2.078	2.287	9.168
FF maximum power	W	4062.159	2396.397	2584.2	7.267
VTOL maximum power	W	11,322.224	7038.022	7704.0	8.645
Transition time	s	22.720	23.160	24.272	4.581

When comparing the error between the sizing result and the conceptual design result, the error for all parameters was within 10%. Table 9 shows that the initial sizing result did not satisfy the design requirements. This is because, as mentioned above, the initial point was determined in a design space that satisfied only the performance requirements defined by MCA. On the contrary, the sizing result satisfied all the design requirements. Figure 16 shows the initial point and the optimum point.

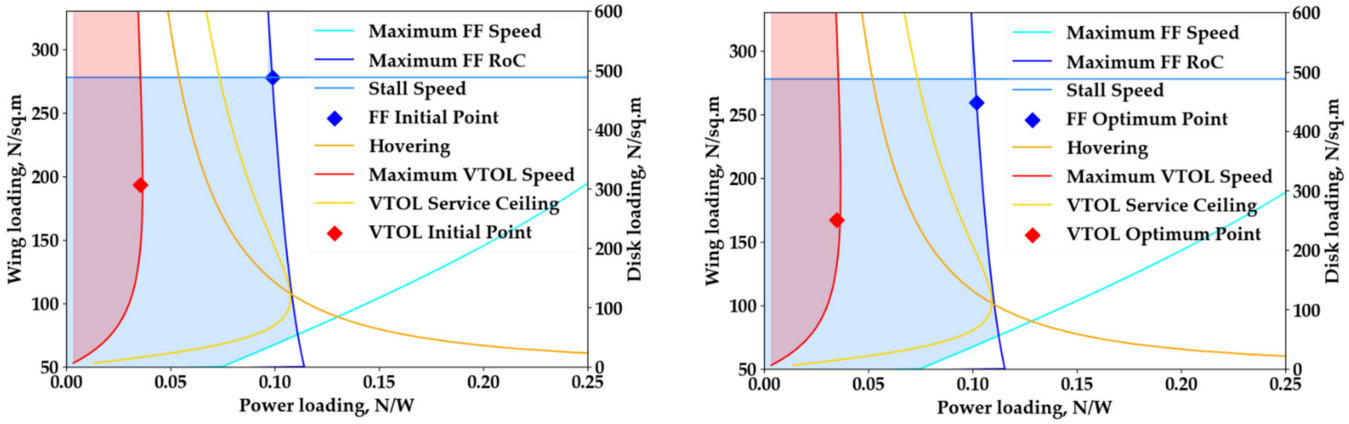

Figure 16. Initial point and optimum point in the design space defined by MCA. (**a**) is the initial point to minimize the wing span and FF/VTOL required power; (**b**) is the optimal point that minimize MTOW of UAV and satisfied all design requirements.

Figure 16 shows that the optimum point shifted to a point that could minimize the MTOW while satisfying the design requirements within the design space defined by MCA through the optimization process. Figure 17 shows the configuration change in each stage of the concept sketch, sizing, and conceptual design. In the sizing result, only the AR, area, and span of the wing are given, so it is a rectangular wing shape. In the conceptual design stage, ADSP is used to optimize geometry parameters such as the sweep angle and taper ratio of the wing.

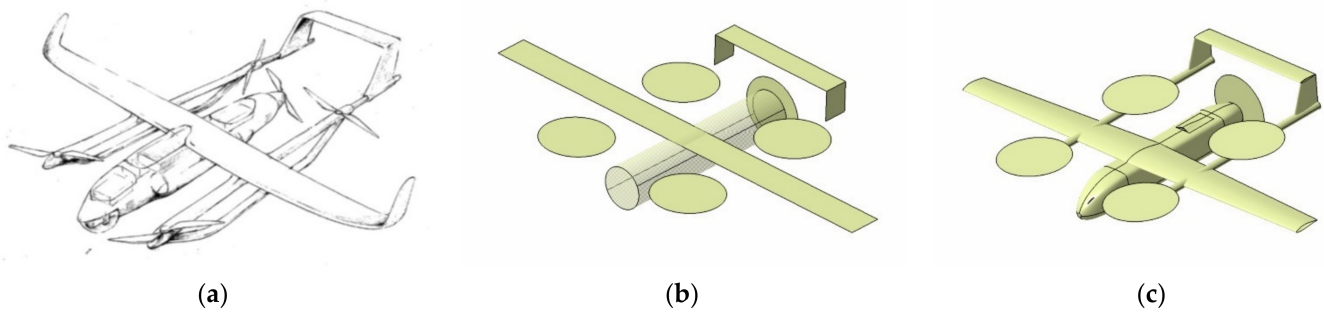

Figure 17. Configuration change of each design stage: (**a**) concept sketch of multi-mode UAV [39]; (**b**) sizing results that include tail sizing results; (**c**) optimum configuration optimized by ADSP.

9.2. EPS Sizing Result

For the sizing result of the EPS, the accuracy of the sizing was analyzed by comparing the mass of the motor, ESC, and propeller applied to the actual UAV and the HFC data, which was developed by Nexcoms. Table 10 shows the comparison of the motor, ESC, and propeller sizing results with the actual mass data.

In the conceptual design process, the FF motor was selected according to the maximum power required in the FF mode, motor weight, and *Kv* predicted in sizing, and the VTOL motor was selected according to the maximum power required in the VTOL mode and the motor weight. After that, the appropriate ESC and propeller for the motor were selected. In the process of selecting a motor with the most similar *Kv* while satisfying the maximum required power for each flight mode and motor weight calculated from the sizing result, it may not be possible to find a motor that satisfies them all, and an error occurs in this process. Errors may occur in other components as well. However, the error for all components between the actual data and the sizing result was within 10%, which means that the accuracy of the sizing method through the regression model developed in

this paper was high and the parameters constituting the regression model were appropriate. For the HFC, the data of the HFC developed by Nexcoms in Figure 18a and the sizing result were compared.

Table 10. Comparison of motor, ESC, propeller sizing results, and actual data.

	Unit	Sizing Results	Actual Data	Error (%)	Remarks
FF motor	kg	0.544	0.555	1.982	T-Motor AT7215 KV245 [21]
FF motor Kv		258.97	245.0	5.702	T-Motor AT7215 KV245 [21]
FF ESC	kg	0.068	0.074	8.284	T-Motor Flame 60A HV [21]
FF propeller	kg	0.097	0.096	0.531	APC 20*10e [26]
VTOL motor	kg	0.371	0.355	4.555	T-Motor V605 KV210 [21]
VTOL ESC	kg	0.071	0.074	4.054	T-Motor Flame 60A HV [21]
VTOL propeller	kg	0.045	0.048	6.583	T-Motor V 22*74 [21]

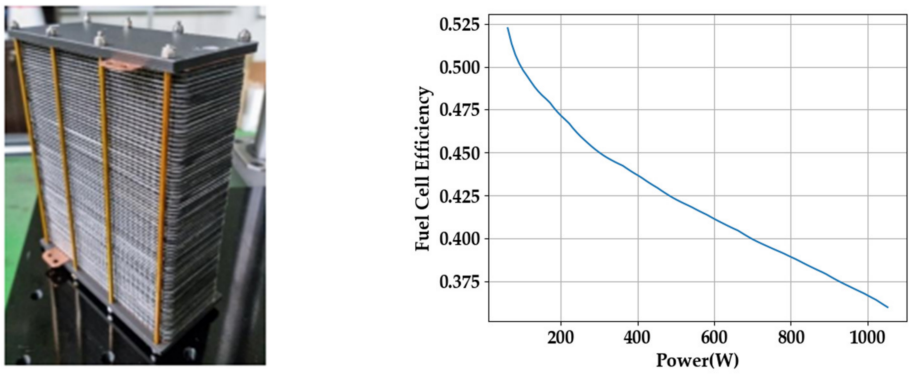

(**a**) (**b**)

Figure 18. (**a**) Nexcoms HFC [38] and the (**b**) efficiency of HFCs according to the HFC's operating power, which is one of the results of sizing.

Table 11 shows the comparison of the HFC sizing results and Nexcoms' HFC's actual data. The HFC sizing was based on the single-cell polarization curve of the Nexcoms HFC, and the error is under 10% for all parameters, which means that the HFC sizing methodology proposed in this paper is very accurate. Figure 18b is one of the results of HFC sizing, which is a graph showing the efficiency according to the operating power of the HFC. It is used for hydrogen tank sizing in mission analysis. Since the efficiency of a hydrogen fuel cell decreases as the power required increases, as shown in Figure 18b, two HFCs were therefore used to lower the power requirement and increase the efficiency in this project.

Table 11. Comparison of HFC sizing results and actual data that was developed by Nexcoms [38].

	Unit	Sizing Results	Actual Data	Error (%)
HFC mass	kg	1.627	1.5	8.483
Stack mass	kg	1.313	1.2	9.417
Cooling fan mass	kg	0.314	0.3	4.747
Control board mass	kg	0.25	0.25	N/A

9.3. Mission Analysis and Transition Analysis Result

As for the result of the mission analysis, the accuracy of the methodology was verified by comparing the sizing result of the required power for each mission segment with the mission analysis result through ADSP. Figure 19 shows the sizing result for the required power for each mission segment and the mission analysis result through ADSP.

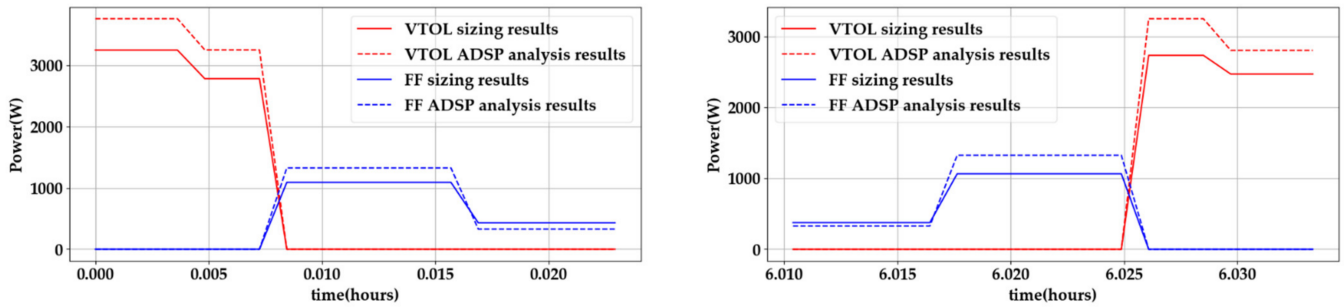

Figure 19. Required power of each mission segment: (**a**) the required power from vertical take-off to cruising; (**b**) the required power from cruising to vertical landing.

The ADSP mission analysis is highly accurate because it uses the results of aerodynamic analysis through the CFD and wind tunnel test results of the electric propulsion system. In addition, because the maximum error in each mission segment was calculated to be approximately 15%, this means that the sizing result was relatively accurate. Figure 20 shows the results of the transition analysis.

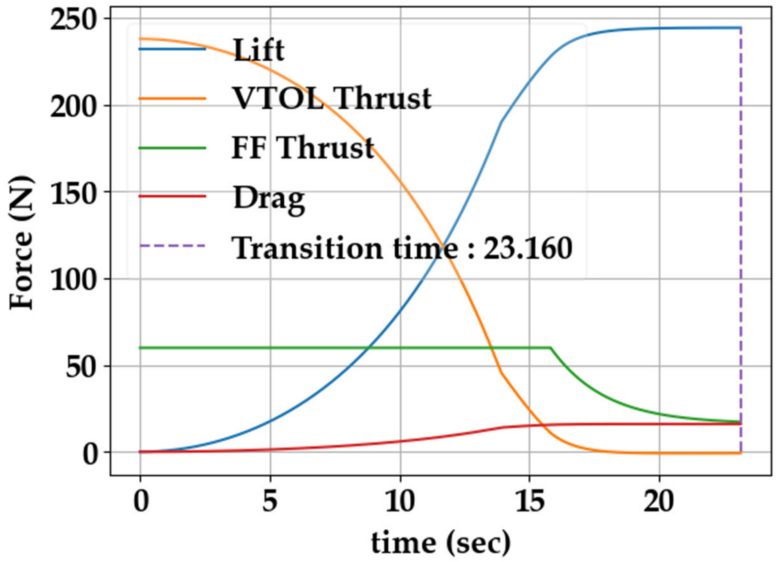

Figure 20. Transition analysis result. This result shows the forces acting on the UAV during its transition. The transition time calculated through analysis satisfied the design requirement as 23.16 s.

Through the transition analysis results, the methodology proposed in Section 6.2 satisfies all the assumptions for transition, and it is possible to predict the transition end time and required power during transition for battery and hydrogen tank sizing. The transition end time was predicted to be 23.16 s. And Figure 21 shows the change in lift sharing, speed, and angle of attack during the transition of the UAV as one of the results of transition analysis.

As mentioned in Section 6.2, the lift presented by the guide control of lift sharing could not be generated at the beginning of the transition due to the insufficient forward speed. Therefore, the angle of attack was maintained at the maximum as shown in Figure 21c, and the lift sharing was performed as Figure 21a. After the forward speed was sufficiently increased, the UAV generated the lift force presented by the guide control, and the angle of attack decreased accordingly and converged to the trim angle of attack in the terminal condition. Table 12 shows the comparison of the battery and hydrogen tank sizing results

and the battery and hydrogen tank data applied to the actual UAV through the calculation of the required power for each mission segment.

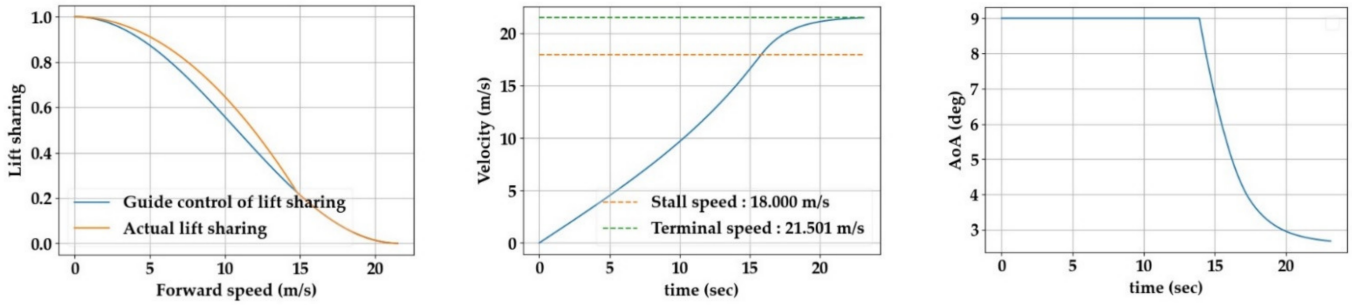

(**a**) (**b**) (**c**)

Figure 21. Transition analysis results: (**a**) shows the comparison of the guide control of lift sharing and actual lift sharing; (**b**) shows the speed change of the UAV during transition; (**c**) shows the angle of attack change of the UAV during transition.

Table 12. Comparison of battery and hydrogen tank sizing results and actual data.

	Unit	Sizing Results	Actual Data	Error (%)
Battery mass	kg	0.558	0.575	3.039
Battery capacity	mAh	3725.581	3800.0	1.958
Hydrogen tank mass	kg	5.599	5.3	5.633
Hydrogen mass	g	244.990	268.2	8.654
Hydrogen tank volume	L	11.839	13	8.928

The battery applied to the UAV was two packs of the EP Power 22.2 V 3800 mAh 55C model [33], and the hydrogen tank was the CTS Ultralight 13 L Type 4 model [40]. The error between the sizing results and actual data of the battery and hydrogen tank was under 10% for all parameters, which means that the battery and hydrogen tank sizing methodology based on the regression model proposed in this paper was accurate.

10. Conclusions

This research presented an improved sizing methodology for a multi-mode eVTOL UAV using a hydrogen fuel cell and Li-po battery. Sizing involved five major procedures. First, the MCA added the performance requirements of the VTOL mode through disk loading so that it can be applied to the multi-mode eVTOL in the existing constraints analysis. Second, for EPS sizing, a sophisticated regression model with an R-squared error of 0.9 or more was built through the data of the existing UAV propulsion component. Through this, the motor, ESC, and propeller sizing methodology was presented, and in the case of the HFC, a sizing technique using the polarization curve of a single cell was presented. Third, mission analysis presented a method of sizing the capacity and weight of the Li-po battery and the weight and volume of the hydrogen tank through the required power defined for each mission segment, and it also presented a new analysis method for the transition mode. The fourth total mass calculation calculated the MTOW of the UAV and performed fixed-point iteration until the MTOW converged. Finally, an optimization method for optimizing the wing loading, power loading, disk loading, and AR was presented so that the sizing result satisfied all the design requirements.

To verify the accuracy of the sizing methodology presented in this paper, the sizing of a 25 kg hydrogen fuel cell UAV was performed. The accuracy of the sizing was verified through comparison with the conceptual design results performed using ADSP based on the sizing results. As a result of the sizing, the MTOW was minimized at 24.91 kg while satisfying all the design requirements. Since the propulsion system selects the product with

the closest performance based on the parameters calculated in sizing during the conceptual design process, errors may occur in the sizing result. In addition, because the geometry data of the UAV wing uses the sizing result as the initial configuration in the conceptual design process and is optimized in consideration of stability, errors may occur with the sizing result. Nevertheless, all the parameters had an error of less than 10% compared with the conceptual design results, which means that the sizing methodology presented in this paper is very accurate and sufficient to be used as initial design data. Therefore, the sizing methodology presented in this paper is a useful tool in the design of UAVs using hydrogen fuel cells and batteries, and if the regression model is replaced with one on a larger scale, it can be usefully for the sizing of urban air mobility (UAM) vehicles.

Author Contributions: Conceptualization, J.-H.A., M.T. and J.-W.L.; Data curation, J.-H.A.; Formal analysis, J.-H.A.; Funding acquisition, J.-W.L.; Investigation, J.-H.A.; Methodology, J.-H.A., M.T. and J.-W.L.; Project administration, J.-W.L.; Software, J.-H.A. and D.-Y.K.; Supervision, M.T. and J.-W.L.; Validation, J.-H.A. and D.-Y.K.; Visualization, J.-H.A.; Writing—Original draft, J.-H.A.; Writing—Review and editing, J.-H.A., K.-S.J., M.T. and J.-W.L. All authors have read and agreed to the published version of the manuscript.

Funding: This research was partially supported by The Project of Conversion by the Past R & D Results through the Ministry of Trade, Industry, and Energy (MOTIE) (P0011388, 2019) and also partially supported by the Basic Science Research Program through the National Research Foundation of Korea (NRF) funded by the Ministry of Education (No. 2020R1A6A1A03046811, 2020).

Institutional Review Board Statement: Not applicable.

Informed Consent Statement: Not applicable.

Acknowledgments: The authors thank Chi Hong Ju, Se Wan Park, and Jong Dae Lee and his team at Nexcoms Co., Ltd., for developing and providing the hydrogen fuel cell data.

Conflicts of Interest: The authors declare no conflict of interest.

References

1. Ian, E. *High-Energy Battery Technologies*; The Faraday Institution: Oxford, UK, 2020.
2. Joey, H. Fuel Cell and Battery Hybrid System Optimization: Towards Increased Range and Endurance. Master's Thesis, Delft University of Technology, Delft, The Netherlands, 2018.
3. Mugin EV350 Full Electric VTOL UAV ARF—Mugin UAV. Available online: https://www.muginuav.com/product/mugin-ev350-full-electric-vtol-uav-arf/ (accessed on 13 October 2021).
4. Foxtech Nimbus Vertical Take-Off and Landing Airplane. Available online: https://www.foxtechfpv.com/foxtech-nimbus-vtol-v2.html (accessed on 13 October 2021).
5. Bell APT. Available online: https://www.bellflight.com/products/bell-apt (accessed on 13 October 2021).
6. Kadhiresan, A.R.; Duffy, M.J. Conceptual Design and Mission Analysis for eVTOL Urban Air Mobility Flight Vehicle Configurations. In Proceedings of the AIAA Aviation 2019 Forum, Dallas, TX, USA, 17–21 June 2019. [CrossRef]
7. Ng, W.; Datta, A. Hydrogen Fuel Cells and Batteries for Electric-Vertical Takeoff and Landing Aircraft. *J. Aircr.* **2019**, *56*, 1765–1782. [CrossRef]
8. Thirkell, A.; Chen, R.; Harrington, I. *A Fuel Cell System Sizing Tool Based on Current Production Aircraft*; SAE Technical Paper; SAE International: Warrendale, PA, USA, 2017. [CrossRef]
9. Bradley, T.; Moffitt, B.; Fuller, T.; Mavris, D.; Parekh, D. Design Studies for Hydrogen Fuel Cell Powered Unmanned Aerial Vehicles. In Proceedings of the 26th AIAA Applied Aerodynamics Conference, Honolulu, HI, USA, 18–21 August 2008. [CrossRef]
10. Raymer, D.P. *Aircraft Design: A Conceptual Approach*, 6th ed.; AIAA Education Series; American Institute of Aeronautics and Astronautics, Inc.: Reston, VA, USA, 2018; ISBN 978-1-62410-490-9.
11. Roskam, J. Rapid sizing method for airplanes. *J. Aircr.* **1986**, *23*, 554–560. [CrossRef]
12. Gudmundsson, S. *General Aviation Aircraft Design: Applied Methods and Procedures*, 1st ed.; Butterworth-Heinemann: Oxford, UK; Waltham, MA, USA, 2014; ISBN 978-0-12-397308-5.
13. Tyan, M.; Nguyen, N.V.; Kim, S.; Lee, J.-W. Comprehensive preliminary sizing/resizing method for a fixed wing—VTOL electric UAV. *Aerosp. Sci. Technol.* **2017**, *71*, 30–41. [CrossRef]
14. *NETL Seventh Edition Fuel Cell Handbook*; National Energy Technology Laboratory: Pittsburgh, PA, USA; Morgantown, WV, USA, 2004.

15. Swider-Lyons, K.; Stroman, R.; Rodgers, J.; Edwards, D.; Mackrell, J.; Schuette, M.; Page, G. Liquid Hydrogen Fuel System for Small Unmanned Air Vehicles. In Proceedings of the 51st AIAA Aerospace Sciences Meeting including the New Horizons Forum and Aerospace Exposition, Grapevine, TX, USA, 7–10 January 2013. [CrossRef]
16. Sadraey, M.H. *Aircraft Design: A Systems Engineering Approach*; Aerospace Series; Wiley: Chichestet, UK, 2013; ISBN 978-1-119-95340-1.
17. Roskam, J. *Methods for Estimating Drag Polars of Subsonic Airplanes*; The University of Kansas: Lawrence, KS, USA, 1971.
18. Filippone, A. *Flight Performance of Fixed and Rotary Wing Aircraft*, 1st ed.; Elsevier Aerospace Engineering Series; Butterworth-Heinemann: Amsterdam, The Netherlands; Boston, MA, USA, 2006; ISBN 978-0-7506-6817-0.
19. Serrano, A.R. Design methodology for hybrid (VTOL + Fixed Wing) unmanned aerial vehicles. *Aeronaut. Aerosp. Open Access J.* **2018**, *2*, 165–176. [CrossRef]
20. Gill, R.; D'Andrea, R. Propeller thrust and drag in forward flight. In Proceedings of the 2017 IEEE Conference on Control Technology and Applications (CCTA), Mauna Lani Resort, HI, USA, 27–30 August 2017; pp. 73–79.
21. T-Motor. Available online: https://uav-en.tmotor.com/ (accessed on 13 October 2021).
22. SciPy Documentation—SciPy v1.7.1 Manual. Available online: https://docs.scipy.org/doc/scipy/reference/ (accessed on 13 October 2021).
23. Scorpion Power System. Available online: https://www.scorpionsystem.com/ (accessed on 13 October 2021).
24. Hacker Motor. Available online: https://hackermotorusa.com/ (accessed on 13 October 2021).
25. Hobbywing Technology Co., Ltd. Available online: https://www.hobbywing.com/ (accessed on 13 October 2021).
26. APC Propellers. Available online: https://www.apcprop.com/ (accessed on 13 October 2021).
27. Hydrogen and Fuel Cell Technologies Office Multi-Year Research, Development, and Demonstration Plan. Available online: https://www.energy.gov/eere/fuelcells/articles/hydrogen-and-fuel-cell-technologies-office-multi-year-research-development (accessed on 13 October 2021).
28. Hes Energy Systems. Available online: https://www.hes.sg/ (accessed on 13 October 2021).
29. Intelligent Energy. Available online: https://www.intelligent-energy.com/ (accessed on 13 October 2021).
30. Doosan Mobility Innovation. Available online: http://www.doosanmobility.com/en/ (accessed on 13 October 2021).
31. Kadyk, T.; Winnefeld, C.; Hanke-Rauschenbach, R.; Krewer, U. Analysis and Design of Fuel Cell Systems for Aviation. *Energies* **2018**, *11*, 375. [CrossRef]
32. Donateo, T.; Ficarella, A.; Spedicato, L.; Arista, A.; Ferraro, M. A new approach to calculating endurance in electric flight and comparing fuel cells and batteries. *Appl. Energy* **2017**, *187*, 807–819. [CrossRef]
33. Falconshop—Various Li-Po Battery. Available online: https://www.falconshop.co.kr/shop/main/index.php (accessed on 13 October 2021).
34. Gundlach, J. *Designing Unmanned Aircraft Systems: A Comprehensive Approach*; AIAA: Reston, VA, USA, 2011; ISBN 978-1-60086-843-6.
35. Nguyen, N.-V.; Choi, S.-M.; Kim, W.-S.; Lee, J.-W.; Kim, S.; Neufeld, D.; Byun, Y.-H. Multidisciplinary Unmanned Combat Air Vehicle system design using Multi-Fidelity Model. *Aerosp. Sci. Technol.* **2013**, *26*, 200–210. [CrossRef]
36. Kim, J.; Nguyen, N.V.; Lee, J.-W. Design Method for Electric Powered Aircraft. In Proceedings of the 5th Asia-Pasific Conference on Systems Engineering, Seoul, Korea, 19–21 October 2011.
37. Konkuk University. *Configuration Design Descriptions (CCD) for Very Light Aircraft (VLA) Development*; Konkuk University: Seoul, Korea, 2011.
38. Joo, C.H. *Nexcoms' Fuel Cell Experimetal Data*; Nexcoms Co., Ltd.: Daejeon, Korea, 2021.
39. *Multi-Mode eVTOL UAV Concept Sketch*; Yuja Arts: Seoul, Korea, 2020.
40. CTS Cylinder-13L 300bar. Available online: http://www.ctscyl.com/prodotti/h2/cts-ultralight-13-0l-300-bar-h2/?lang=en (accessed on 13 October 2021).